Dyes and Pigments 84 (2009) 88–94

Contents lists available at ScienceDirect

Dyes and Pigments

journal homepage: www.elsevier.com/locate/dyepig

The synthesis and characterization of 2-(2′-pyridyl)benzimidazole heteroleptic ruthenium complex: Efficient sensitizer for molecular photovoltaics

Cigdem Sahin [a,b], Mahmut Ulusoy [c], Ceylan Zafer [a], Cihan Ozsoy [a], Canan Varlikli [a,*], Thomas Dittrich [d], Bekir Cetinkaya [c], Siddik Icli [a]

[a] Solar Energy Institute, Ege University, 35100 – Bornova, Izmir, Turkey
[b] Chemistry Department, Art & Science Faculty, Pamukkale University, Denizli, Turkey
[c] Chemistry Department, Science Faculty, Ege University, 35100 – Bornova, Izmir, Turkey
[d] Helmholtz Centre Berlin for Materials and Energy-Berlin, Germany

ARTICLE INFO

Article history:
Received 4 February 2009
Received in revised form
23 June 2009
Accepted 24 June 2009
Available online 5 July 2009

Keywords:
Ruthenium (II) complex
2-(2′-pyridyl)benzimidazole
Charge-separation
Titanium dioxide
Surface photovoltage spectroscopy
Dye sensitized solar cells

ABSTRACT

The novel ligand 1-(2,4,6-trimethylbenzyl)-2-(2′-pyridyl)benzimidazole and its heteroleptic ruthenium (II) complex were synthesized. The complex was characterized using spectroscopic methods and cyclic voltammetry. Charge-separation was investigated within nanoporous titanium dioxide employing surface photovoltage spectroscopy. The performance of the ruthenium complex as a charge transfer photosensitizer in nanocrystalline, titanium dioxide-based, dye sensitized solar cells was studied under standard AM 1.5 sunlight using an electrolyte consisting of 0.6 M 1-butyl-3-methyl-imidazolium iodide, 0.1 M lithium iodide, 0.05 M iodine and 0.5 M 4-*tert*-butyl pyridine in 3-methoxy propyonitrile. The novel complex had a photocurrent density of 9.47 mA cm^{-2}, 600 mV open circuit potential and 0.60 fill factor yielding an efficiency of 3.4%. The photovoltaic performance of the colorant was compared with that of *cis*-bis(isothiocyanato)(2,2'-bipyridyl-4,4'-dicarboxylato) (2,2'-bipyridyl-4,4'-di-nonyl) ruthenium(II); both compounds exhibited similar efficiency, while the fill factor value was higher for the novel dye.

1. Introduction

Nanocrystalline titanium dioxide (nc-TiO_2) based dye sensitized solar cells (nc-DSCs) convert sunlight to electricity and has enjoyed much interest recently [1]. The advantages of these devices include high photoelectrical conversion efficiency over a large part of the visible light spectrum under direct sunlight and low manufacturing costs compared to traditional solid state, crystalline silicon solar cells [2,3]. The working principle of nc-DSC's is based on photoelectrochemistry: the photosensitizers are excited by incoming photons at the TiO_2/electrolyte interface and the ensuing, excited charge carriers (i.e. electrons) are injected into the TiO_2 conduction band; the dye is reduced by electrolyte including a redox couple which is usually iodine/triiodide regenerated [4].

Ruthenium (II) complexes that contain a benzimidazole ligand have important applications in optoelectronic devices because of their chemical and physical properties [5,6]. These compounds enjoy usage in electrogenerated chemiluminescence (ECL) systems [7], nc-TiO_2 based dye sensitized solar cells (nc-DSCs) [6], and organic light-emitting diodes (OLEDs) [5]. In recent years, among π-conjugated molecules, those containing electron-deficient benzene-fused five-membered heteroaromatic rings with nitrogen atom(s), benzimidazole derivatives as ligand have been widely employed as acceptor moieties in various optoelectronic materials [8]. Such ligands also demonstrate conjugated character to explore efficient electron or energy transfer. The benzimidazol ring is connected to the $C_6H_2(CH_3)_3$ arene by a methylene bridge, which leads to a system with very little apparent strain [9]. The strain in coordination compounds may influence the stability, reactivity, spectroscopic and electrochemical properties [10]. Furthermore, the group of 2,4,6-trimethylbenzyl increases the solubility of the ruthenium complex. Our aim in synthesis of a heteroleptic ruthenium (II) complex containing benzimidazole ligand and investigating its photoelectrochemical activity is to enhance the spectral response over a wide wavelength region, maintain a sufficient thermodynamic driving force for electron injection from LUMO level of dye molecules to conduction band of TiO_2 and electron transfer from electrolyte to the oxidized sensitizer [11,12].

The present paper concerns the synthesis and characterization of a novel, heteroleptic ruthenium (II) complex that contains a benzimidazole ligand; the compound's photovoltaic properties

* Corresponding author. Tel.: +90 232 3884000/1244; fax: +90 232 3886027.
E-mail address: canan.varlikli@ege.edu.tr (C. Varlikli).

0143-7208/$ – see front matter © 2009 Elsevier Ltd. All rights reserved.
doi:10.1016/j.dyepig.2009.06.016

are compared to those of *cis*-bis(isothiocyanato) (2,2'-bipyridyl-4,4'-dicarboxylato) (2,2'-bipyridyl-4,4'-di-nonyl) ruthenium(II), i.e. Z907, as photosensitizer in nc-DSC's.

2. Experimental

2.1. Materials

Dichloro(*p*-cymene) ruthenium(II) dimer (caution: irritant; incompatible with oxidizing agents, halogens and active metals), ammonium thiocyanate, tetrabutyl ammonium hexafluorophosphate ($TBAPF_6$) (caution: corrosive to skin, eyes and respiratory tract; incompatible with oxidizing agents and active metals), nitric acid and acetic acid were purchased from Fluka. Hydrogen hexachloroplatinate (IV) solution (caution: may decompose when exposed to light; moisture sensitive; incompatible with light, moist air or water, strong oxidizing agents and bases), ethyl cellulose, LH-20 Sephadex gel (crosslinked dextran-based resin) and 4,4′-dimethyl-2,2′-bipyridine were obtained from Aldrich. Titanium tetra iso-propoxide [$Ti(OPr^i)_4$] (caution: moisture sensitive, forming low flash point mixture; incompatible with many acids, bases, aliphatic amines) was obtained from Acros. Z907 and nc-TiO_2 porous anatase paste was purchased from Solaronix. All reactions and manipulations of air-sensitive materials were carried out under nitrogen atmosphere using standard Schlenk techniques. Solvents were dried and freshly distilled prior to use. All other chemicals were used as received. The summary of synthetic procedure and open structure of the synthesized complex, namely CS23 is given in Fig. 1.

2.2. Analytical measurements

UV–Vis spectra were recorded in a 1 cm path length quartz cell by using Analytic Jena S 600 UV spectrophotometer. Infrared spectra were obtained with a Perkin Elmer, Spectrum BX-FTIR spectrophotometer, electrochemical data were obtained by using a CH Instrument 660 B Model Electrochemical Workstation. NMR spectra were recorded at 297 K on a Varian Mercury AS 400 NMR instrument at 400 MHz (^1H), 100.56 MHz (^{13}C). Coupling constants *J* are given in Hz. Melting points were determined using an Electrothermal 9100 melting point detection apparatus. The thickness of the TiO_2 films that were used in surface photovoltage (SPV) measurements was obtained by using Scanning electron microscope (SEM), LEO 1530 with Gemini column. While the thickness of the nc-TiO_2 layers used in nc-DSC preparation were measured with the use of a surface profilometer, Ambios XP-1. Photovoltaic data were obtained by using Keithley 2400 source-meter and Labview data acquisition system.

2.3. Surface photovoltage spectroscopy

nc-TiO_2 layers were prepared by spin coating nc-TiO_2 porous anatase paste at 2000 rpm for 30 s on SnO_2:F coated glass. Coated electrodes were sintered at 450 °C for 30 min. The thickness of the TiO_2 film was about 100 nm TiO_2 layers were soaked in dye solutions of Z907 and CS23 [3×10^{-5} M in N,N-dimethylformamide (DMF)] for 30 min.

SPV spectra were measured in the capacitor arrangement with a semitransparent Cr electrode deposited on a quartz cylinder and mica as a spacer using by light chopped at a frequency of 5 Hz. Dye adsorbed TiO_2 layers were investigated with a halogen lamp (250 W) and a quartz prism monochromator. The measurements were performed in Argon (600 mbar) atmosphere at room temperature.

2.4. Synthesis of 4,4′-dicarboxy-2,2′-bipyridine (L_1)

Starting from 4,4′-methyl-2,2′-bipyridine, L_1 was synthesized according to literature [13]. The yield was 96%. FTIR (KBr, cm^{-1}): 3449, 3114, 2442, 1719, 1366, 1290, 1268, 1244, 766, 682. ^1H NMR (D_2O + NaOH) δ ppm: 7.73 (d, J = 5.2, 2H, CC*H*CH); 8.24

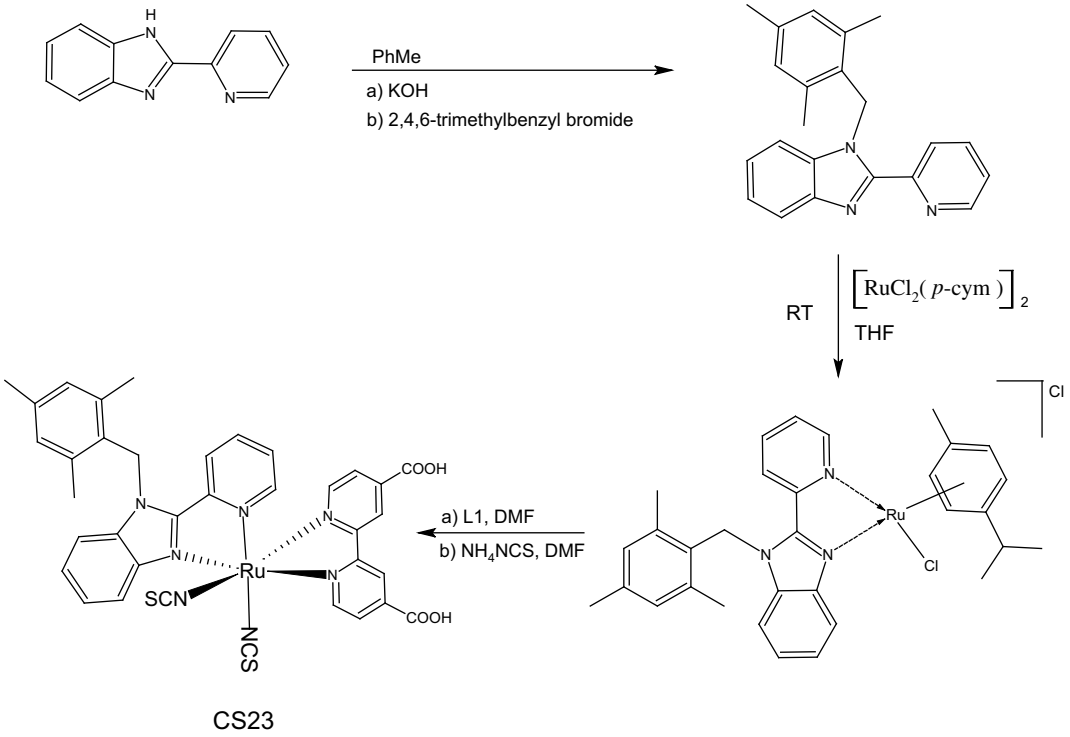

Fig. 1. Synthetic route followed in the synthesis of CS23.

(s, 2H, CC*H*C); 8.64 (d, J = 5.2, 2H, NC*H*CH). ^{13}C NMR (D_2O + NaOH) δ ppm: 121.5; 123.5; 146.6; 149.9; 155.9; 173.2.

2.5. Synthesis of 1-(2,4,6-trimethylbenzyl)-2-(2′-pyridyl)benzimidazole (L_2)

KOH (616 mg, 11.0 mmol) was added to a solution of 2-pyridylbenzimidazole (1.95 g, 10.0 mmol) in toluene (10 mL) and stirred at reflux for 8 h. 2, 4,6-trimethylbenzyl bromide (2.13 g, 10.0 mmol) was added into this reaction mixture and then heated under reflux for 12 h. The volatiles were evaporated in vacuum to dryness. The residue was dissolved in CH_2Cl_2 and filtered via cannula on celite. The solution was concentrated to 15 mL and then the desired product was precipitated in 30 mL hexane. The off-white solid was obtained with 85% yield. M.p. 170–172 °C. ^{1}H NMR ($CDCl_3$) δ ppm: 2.15 (s, 6H, mes-(C*H*$_3$)$_2$); 2.26 (s, 3H, mes-C*H*$_3$); 6.22 (s, 2H, N–C*H*$_2$); 6.76 (d, J = 8.0 Hz, 1H); 6.83 (s, 2H, mes(C*H*)$_2$); 7.03–7.07 (m, 1H); 7.20–7.35 (m, 2H); 7.85–7.89 (m, 2H); 8.44–8.46 (dd, J = 8.0, 8.4 Hz, 1H); 8.70–8.72 (m,1H). ^{13}C NMR ($CDCl_3$) δ ppm: 20.4; 21.1; 46.1; 112.0; 120.1; 122.8; 123.6; 124.1; 125.7; 129.6; 129.9; 136.4; 137.3; 137.5; 137.7; 142.4; 148.6; 150.7; 151.0.

2.6. Synthesis of [Ru(L_2)(p-cymene)Cl][Cl] (MU610)

Ru-*p*-cymene dimer (306 mg, 0.5 mmol) was added to a THF solution (8 mL) of L_2 ligand (327 mg, 1.0 mmol). The color of mixture immediately turned from red to yellow. The reaction mixture was stirred at room temperature for 2 h. The precipitate was filtered off, washed with THF and filtered off again, to remove un-reacted L_2. The residue was dissolved in CH_2Cl_2 (5 mL) and then precipitated with diethyl ether (10 mL) to give the yellow solid with 87% yield. M.p. 183–187 °C. ^{1}H NMR ($CDCl_3$) δ ppm:1.01–1.05 (m, 6H, cym-CH(C*H*$_3$)$_2$); 2.08 (s, 6H, mes-(C*H*$_3$)$_2$); 2.27 (s, 3H, cym-C*H*$_3$); 2.31 (s, 3H, mes-C*H*$_3$); 2.58–2.61 (m, 1H, cym-C*H*CH$_3$); 5.80–5.83 (m, 2H, cym); 5.86–6.00 (m, 2H, cym); 6.11 (d, J = 6 Hz, 1H); 6.22 (d, J = 5.6 Hz, 1H); 6.63 (d, J = 8.8 Hz, 1H); 6.91 (s, 2H, N–C*H*$_2$); 7.23 (d, J = 7.6 Hz, 1H); 7.48 (t, J = 7.4 Hz, 2H); 7.76–7.82 (m, 2H); 8.11 (t, J = 7.6 Hz, 1H); 8.39 (d, J = 8.8 Hz, 1H); 9.71 (d, J = 5.2 Hz, 1H). ^{13}C NMR ($CDCl_3$) δ ppm: 15.5; 19.4; 20.1; 22.5; 34.5; 48.2; 66.1; 80.6; 83.7; 84.3; 86.9; 104.9; 105.1; 113.9; 118.2; 125.3; 125.9; 126.1; 128.3; 130.4; 136.0; 137.8; 139.8; 140.9; 145.9; 149.8; 158.6.

2.7. Synthesis of [RuL_1L_2(NCS)$_2$] (CS23)

MU610 (108 mg, 0.17 mmol) was dissolved in DMF (40 ml) and L_1 (41.6 mg, 0.17 mmol) was added into this solution. The reaction was refluxed under nitrogen for 6 h. Then NH_4NCS (404 mg, 5,3 mmol) addition was performed and the solution was heated at 140 °C for 6 h. Afterwards DMF was evaporated, the resulting residue was suspended in water and the insoluble product was collected on a sintered glass crucible by suction filtration. The solid was washed with distilled water and diethyl ether. The crude complex was purified on Sephadex LH-20 column using methanol as an eluent and then recrystallized from methanol: diethyl ether (5:10) mixture. The yield of CS23 was 45%. FTIR (KBr, cm^{-1}) (Fig. 3): 3447, 3349, 3062, 2919, 2110, 1977, 1714, 1608, 1544, 1479, 1445, 1406, 1232, 750. ^{1}H NMR (CD_3OD) δ ppm (Fig. 2): 1.28 (s, 3H); 2.06 (s, 3H); 2.22 (s, 3H); 6.01 (s, 2H), 6.78 (s, 2H), 6.91 (d, J = 8.4 Hz, 1H); 7.10 (t, J = 8, 7.6 Hz, 1H); 7.23 (t, J = 7.6, 7.2 Hz, 1H); 7.49 (t, J = 7.6, 4.8 Hz, 1H); 7.56 (d, J = 5.2 Hz, 1H); 7.64 (d, J = 5.6 Hz, 1H); 7.70 (d, J = 8.0 Hz, 1H); 7.96 (t, J = 8.0 Hz, 1H); 8.05 (d, J = 7.2 Hz, 1H); 8.21 (d, J = 6.0 Hz, 1H); 8.74 (d, J = 4.8 Hz, 1H); 8.83 (s, 1H); 8.99 (s, 1H); 9.49 (d, J = 6 Hz, 1H).

2.8. Synthesis of TiO_2 nanoparticles and electrode preparation

TiO_2 nano-particles were synthesized by sol–gel method and growth to the 20–25 nm by Ostwald ripening in autoclave. The synthesis was done by modification of procedure reported by Graetzel et al. [14]. 58.6 g Ti(OPr^i)$_4$ was injected into 12 g glacial acetic acid. The solution was added dropwise in to the 290 ml cooled deionized water under vigorous stirring. 5.4 ml nitric acid (65% HNO_3) was added to the colloidal suspension to adjust the pH: 1–2. The sol was peptized at 78 °C for 75 min in oven. Water was added to adjust the colloidal sol volume to 370 ml and than sol was transferred to the Teflon baker equipped autoclave and heated at 235 °C for 12 h for hydrothermal growth of the particles. 2.4 ml nitric acid (65% HNO_3) was added to autoclaved suspension and than concentrated to 16.5% (w/w) TiO_2. All of the remaining water

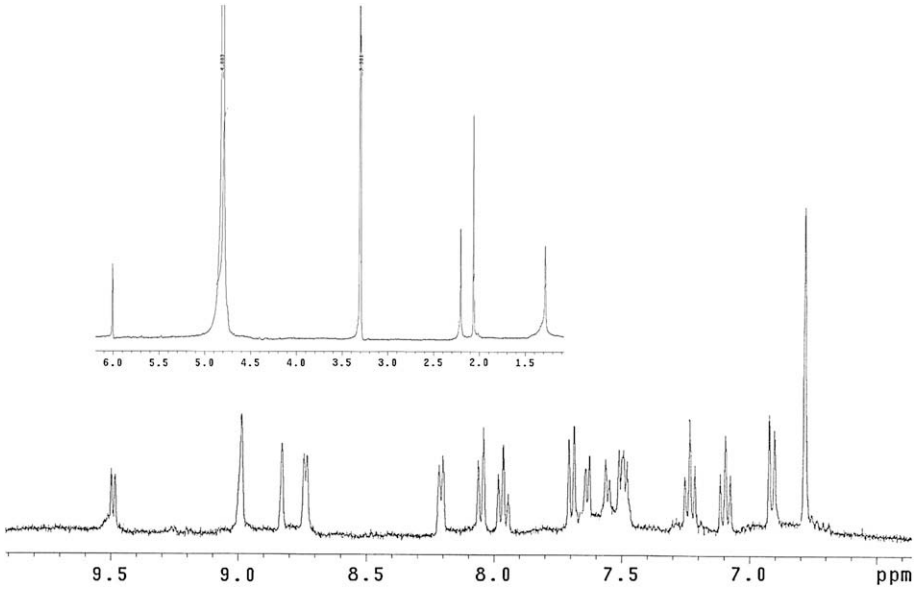

Fig. 2. ^{1}H NMR spectrum of CS23 complex in CD_3OD.

was exchanged with ethanol by centrifuging and 40% (w/w) TiO_2 paste was obtained. 4.5% ethyl cellulose in ethanol and 79 g anhydrous α-terpineol were added and paste was sonicated by ultrasonic horn at 200W power for 10 min. Obtained homogeneous paste was placed to the rotary evaporator to remove ethanol.

The TiO_2 paste was coated on transparent conductive oxide coated glass electrodes (SnO2:F, TEC15, R_{sheet}: 15 ohm/□) by screen printing technique. TiO_2 electrodes first dried at room temperature and than sintered at 450 °C for 1 h with 10 °C/min heating rate. After sintering, aqueous $TiCl_4$ solution was applied on the TiO_2 film and left under water vapor for 30 min at room temperature to obtain a better electrical contact between the nano-particles. Finally TiO_2 electrodes sintered again at 500 °C for 30 min with 10 °C/min heating rate. At the end of the process nano-crystaline mesoporous TiO_2 film with 4 μm thickness was obtained.

2.9. Sensitization with dye and DSC assembly

Sintered electrodes were allowed to cool down slowly. While electrode temperature was around 100 °C, TiO_2 electrodes were immersed in dye solution containing 0.3 mM Z-907 and CS23 dye in acetonitrile:*tert*-butanol (1:1) and DMF overnight. Sensitized TiO_2 electrodes were rinsed with acetonitrile and kept in desiccator. Counter electrode was prepared by thermal reduction of hexachloroplatinic acid to the platinum. 1% (v/v) solution in 2-propanol was used for platinization of FTO coated electrode. Drop casted electrodes annealed at 400 °C for 20 min.

The nc-DSCs were prepared by putting the electrodes on top of each other in sandwich geometry and in the middle and 50 μm thick thermoplastic polymer frame Surlyn® 1702 (DuPont) was placed. The electrodes were sealed by heating around 100 °C and pressing slightly. Electrolyte consisting iodide/triiodide redox couple was filled into cell via pre-drilled small hole by vacuum. The used electrolyte composition was 0.6 M 1-butyl-3-methy-imidazolium iodide (BMII), 0.1 M lithium iodide (LiI), 0.05 M iodine (I_2) and 0.5 M *tert*-butyl pyridine (TBP) dissolved in 3-methoxy propyonitrile (MPN). The active area of the prepared solar cells was adjusted to 1.0 cm^2.

The photovoltaic characterizations of the nc-DSCs were done under the dark and standard conditions (AM 1.5 global radiation with 100 mW/cm^2 light intensity) without using a mask.

The photovoltaic parameters of nc-DSC solar cells were obtained from the following equations.

$$FF = \frac{V_m I_m}{V_{oc} I_{sc}} \quad (1)$$

and

$$\eta = \frac{I_{sc} V_{oc} FF}{P_{in} A} \quad (2)$$

Where FF is filling factor, V_{oc} is the open circuit voltage, I_{sc} is the short current. I_m and V_m are current and potential at maximum power point, respectively. P_{in} is the intensity of incident light, A is the cell active area and η is the efficiency. The efficiency of the photoelectrochemical conversion of absorbed photons was judged by measuring the IPCE % values and by the use of following equation:

$$\text{IPCE} = \left[\frac{1240(\text{eV.nm}) x I(\text{mA/cm}^2)}{\lambda(\text{nm}) X P_{inc}(\text{mXA/cm}^2)}\right] 100 \quad (3)$$

where P_{inc} is the incident light power, which was measured by Nova II versatile laser power energy display at the specific wavelength (λ), and *I* is the produced photocurrent.

3. Results and discussion

3.1. Structural characterization

The compounds are fully characterized by FTIR, ^1H and ^{13}C NMR spectroscopy. The ^1H NMR ($CDCl_3$) spectra of the L_2 show proton signals for the protons from the aryl rings and proton signals at *ca* 2 ppm indicates the presence of the methyl substituents on the aryl rings at 2, 4 and 6 positions. Characteristic signals of benzyl substituents are observed as singlets at 6.22 ppm. The ^{13}C NMR data for ligand is consistent with the proposed structure. In the ^{13}C NMR ($CDCl_3$), methyl and benzylic carbons resonances at 20, 21 and 46 ppm, respectively. In the ^1H NMR ($CDCl_3$) spectra of complex MU610, characteristic signals of cymene aromatic protons are observed as multiplets *ca* 5.80–6.00 ppm. The ^1H NMR ($CDOD_3$) spectra of complex CS23 contain 16 resonance peaks in the aromatic region, and 3 methyl resonance peaks in the aliphatic region (Fig. 2). The singlet peak at 6.00 ppm is due to the benzyl substituent.

Further structural characterization of CS23 was carried out by FTIR spectroscopy. The high resolution spectrum (Fig. 3) exhibits two bands centered at 2110 and 1977 cm^{-1} which are characteristic of the *cis*-configuration for the two thiocyanate ligands [11,15]. Furthermore, the N-coordination of the thiocyanate group is confirmed by the presence of vibrational band at 750 cm^{-1}. The spectra shows strong band at 1714 cm^{-1} due to carboxylic acid groups. The intense peak at 1232 cm^{-1} is assigned to the (C–O) stretching [16,17]. The bands at 1607, 1544, 1479, 1445, 1406 cm^{-1} are due to the ring stretching of the ligands.

3.2. Absorption studies

The absorption spectra of CS23 in DMF and on nc-TiO_2 film are shown in Figs. 4a and b, respectively, and maximum absorption wavelengths and the absorption coefficients are summarized in Table 1. The lowest metal-to-ligand charge transfer (MLCT) absorption band is at 531 nm [18] with a molar extinction coefficient of 4.2×10^3 M^{-1} cm^{-1}. The absorption bands at 267, 336 and 311 nm are assigned to the intra ligand π–π^* transition of L_2 and L_1 ligands, respectively. When compared with Z907, a red shift of 7 nm in the lowest energy MLCT absorption and a decrease in molar extinction coefficient is obtained in CS23. This situation is attributed to the more extensive π-back donation on the L_2 ligand [11].

The absorption spectrum of CS23 anchored on a 4 μm thick nc-TiO_2 electrode gives the low-energy MLCT maximum at 535 nm, which is 4 nm red shifted when compared to the solution phase. This is due to the fact that, on the electrode, the carboxylate groups bind to the TiO_2 surface, in which Ti^{4+} acts as an electron acceptor, which causes a decrease in the LUMO of L_1 [1].

3.3. Electrochemical measurements

The electrochemical studies were performed in a cell containing Ag wire quasi reference electrode, glassy carbon working electrode, Pt wire counter electrode and the used supporting electrolyte consists of 0.1 M $TBAPF_6$ in DMF. The redox potentials are summarized in Table 1. Fig. 5 shows cyclic voltammogram of CS23 in DMF. It shows one irreversible oxidation and two irreversible reduction peaks at +0.99, and −1.29, −1.86 V *vs.* Ag/Ag^+, respectively. The peak at 0.65 V *vs.* Ag/Ag^+ is due to ferrocenium/ferrocene couple, which was used as an internal standard. Oxidation and reduction peaks are assigned to Ru (II) couple and L_1, L_2 ligand, respectively [16]. Several consecutive voltammograms are performed and no significant change in peak currents is observed.

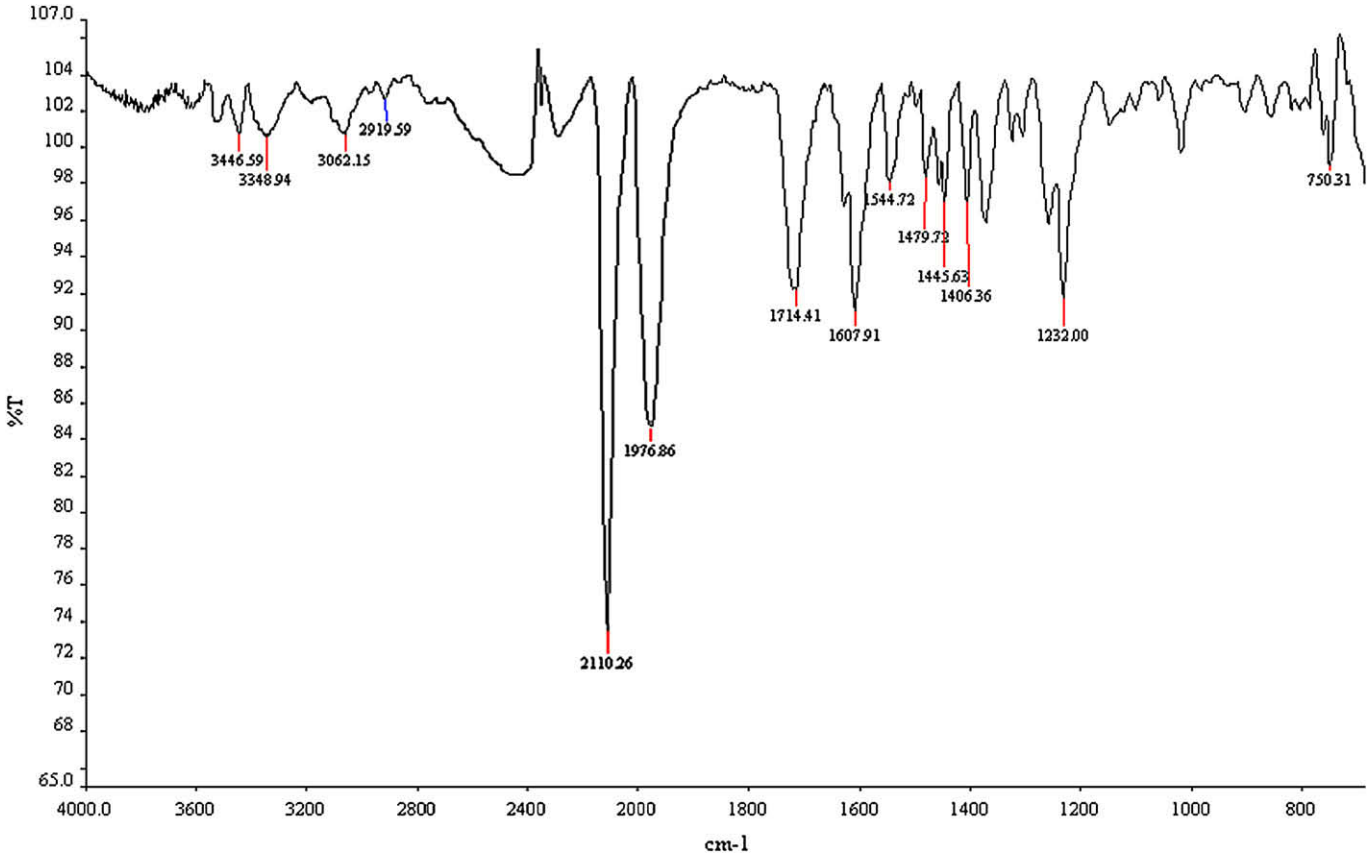

Fig. 3. FTIR spectrum of CS23 complex.

The cyclic voltammogram of CS23 dye anchored on a 4 μm thick TiO_2 shows that the quasi-reversible metal-centered oxidation potential is shifted to anodic area (0.07 V) when compared to the solution phase. This situation is attributed to the interaction of carboxylate groups with the TiO_2 surface [19].

3.4. SPV measurements

Surface photovoltage spectroscopy is a useful technique to investigate charge-separation in porous metal oxide layers that contain dye [20]. Fig. 6 shows the spectra of photovoltage (PV) amplitude of the TiO_2 layers with adsorbed dye for CS23 and Z907. The SPV signals are positive. This points out electron injection from the adsorbed dye molecules into the TiO_2 layer and positive charging of the surface. The onset of electron injection from CS23 dye molecules into TiO_2 layer is identical with Z907. The onset of electron injection is 1.3 eV.

The PV amplitude spectra are very similar for CS23 and Z907. The signal at photon energy around 2.3 eV is larger by about 1.5 times for the TiO_2 layer with adsorbed Z907. This result indicates

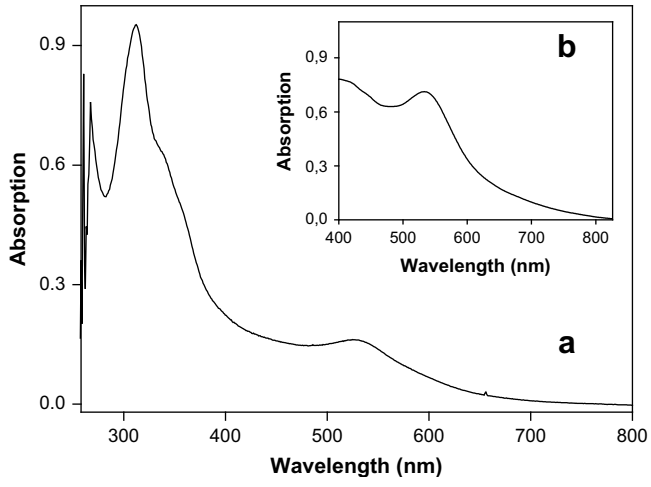

Fig. 4. a) UV–Vis absorption spectra of 4 × 10^{-5} M CS23 solution in DMF b) UV–Vis absorption spectra of CS23 dye adsorbed on 4 μm thick nc-TiO_2 film.

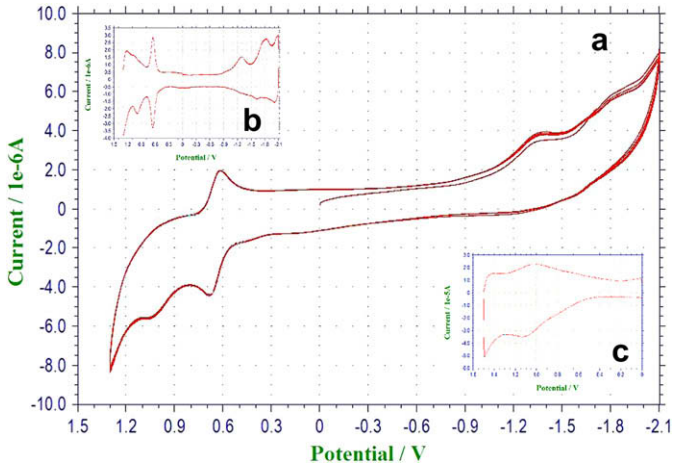

Fig. 5. a) 4 consecutive cyclic voltammograms of CS23 and b) differential of CS23 voltammogram measured in DMF solutions. The couple at 0.65 V *vs.* Ag/Ag^+ is due to ferrocenium/ferrocene couple, which was used as an internal standard. c) cyclic voltammograms of the CS23 dye adsorbed on 4 μm thick nc-TiO_2 film; scan rate is 100 mV^{-1}.

Table 1
Absorption and electrochemical data of the complexes in DMF.

Complex	λ_{max}, (nm) ($\varepsilon/10^4$ M^{-1} cm^{-1})		E_{red1} (V)	E_{red2} (V)	E_{ox} (V)
	$\pi \rightarrow \pi^*$	$d\ \pi \rightarrow \pi^*$			
CS23	267 (1.93) 311 (2.38) 336 (1.58)	531 (0.42)	−1.29	−1.86	0.99
Z907	267 (1.58) 300 (3.48)	374 (0.90) 524 (0.93)	−1.41	−1.72	0.98

a slightly enhanced electron injection from Z907 dye molecules into TiO_2.

3.5. Photovoltaic performance

Fig. 7 shows the incident photon to current conversion efficiency (IPCE) spectra of nc-DSC based on Z907 and CS23 adsorbed from two different solvents, acetonitrile:*tert*-butanol (MeCN:*tert*-BuOH)(1:1) and DMF. Both of the dyes exhibit a maximum at 530 nm. IPCE values of Z907 at 530 nm are 89% and 88% for the cells prepared from MeCN:*tert*-BuOH and DMF solvents, respectively, while for CS23 these values are 79% and 78%, respectively. About 10% IPCE difference between Z907 and CS23 is due to the better electron injection capacity of Z907. The onset wavelength of the IPCE spectrum of CS23 is 750 nm. This value is almost the same with nc-DSC based on Z907. These results are confirmed by SPV measurements. As seen from Fig. 6, SPV spectra exhibit maxima at 2.3 eV which corresponds to 539 nm for both of the dyes and at this wavelength the electron injection from Z907 dye molecules into TiO_2 is slightly higher when compared with CS23.

Current density–Voltage (I–V) curves of nc-DSC sensitized with Z907 and CS23 from their acetonitrile: *tert*-BuOH (MeCN) and DMF solutions are given in Fig. 8 and the photovoltaic performance data are summarized in Table 2. Open circuit voltages (V_{oc}) are almost the same for both dyes adsorbed from the same solvents. nc-DSCs prepared from TiO_2 electrodes sensitized with dye from DMF solution exhibits 10 mV higher V_{oc} than that of sensitized from MeCN: *tert*-BuOH (1:1) solution. This should result from better solubility of the Z907 and CS23 in DMF. Better solubility prevents the formation of aggregates on TiO_2 surface which increases charge recombination and decreases short circuit current and open circuit voltage [21,22]. The energy level of the dye may shift incase of agglomerates on the TiO_2-surface and this may result in different

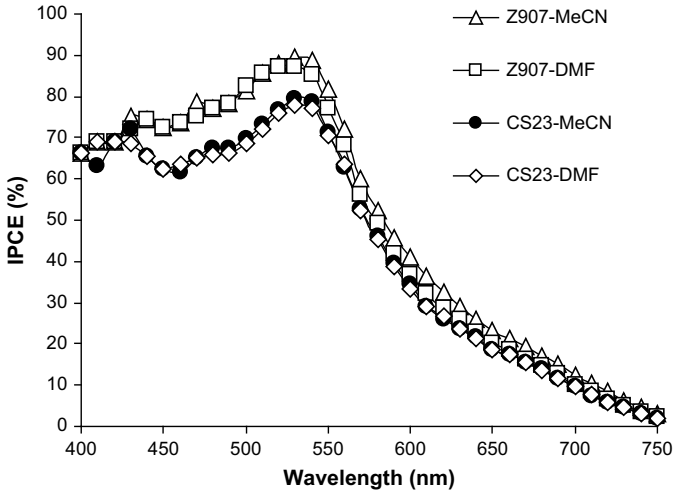

Fig. 7. Incident photon to current conversion efficiency (IPCE) spectra of Z907 and CS23 adsorbed from acetonitrile:*tert*-BuOH (MeCN) and dimethyl fomamide (DMF).

electronic properties of the ground and/or the exited state that may affect the charge injection efficiency [23,24].

Z907 exhibits higher photocurrent than CS23 due to larger IPCE. The I_{sc} obtained from nc-DSC sensitized with Z907 is 11.49 $mAcm^{-2}$ and 11.15 $mAcm^{-2}$ for the cells prepared from MeCN: *tert*-BuOH (1:1) and DMF solutions, respectively, while these values are 9.47 $mAcm^{-2}$ and 9.04 $mAcm^{-2}$, respectively for CS23. Higher electron injection yield from dye LUMO to TiO_2 conduction band (CB) in DSSC sensitized with Z907 yield in higher IPCE. Whereas, fill factor values (FF) are higher in the case of CS23. The FF increases from 0.5 to 0.6 when the sensitizer is changed from Z907 to CS23. The fill factor is strongly affected by charge recombination rate which results in charge transfer resistance in TiO_2/dye/electrolyte interface. Higher charge transfer resistance and higher recombination rate lowers the fill factor. Therefore it may be concluded that charge recombination rate is lower with CS23 sensitizer. This statement is also supported by the SPV spectroscopy results as shown in Fig. 6. With CS23 sensitized TiO_2 electrodes, SPV values are slightly lower when compared with Z907, which indicates slower charge recombination rate [20,25–27].

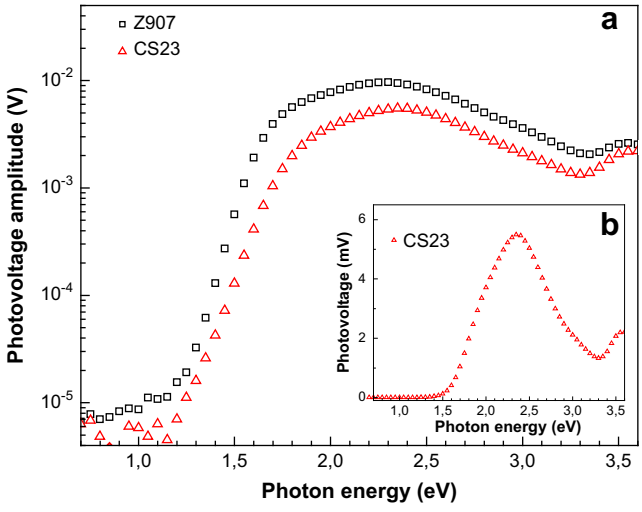

Fig. 6. a) Spectra of the PV amplitude of np-TiO_2 layers with CS23 dye (△) and Z907 dye (□) molecules. b) SPV spectra were measured in the capacitor arrangement under chopped light illumination for TiO_2 layer with CS23 dye in Ar atm.

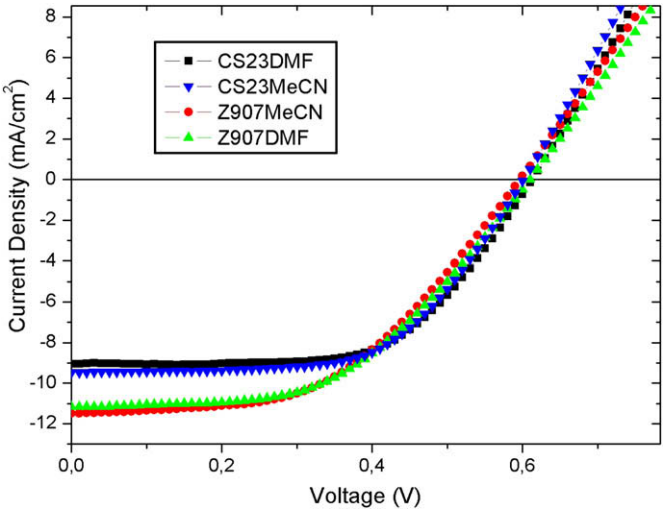

Fig. 8. Current Density–Voltage (I–V) curves of nc-DSC sensitized with Z907 and CS23 from acetonitrile:*tert*-BuOH (MeCN) and DMF.

Table 2
Photovoltaic performances of the DSSCs under 100 m Wcm^{-2} light intensity and AM 1.5 global radiation.

Dye	*Voc* (mV)	Isc (mA/cm^2)	FF	η (%)
Z907–MeCN	600	11.49	0.49	3.40
Z907–DMF	610	11.15	0.50	3.44
CS23–MeCN	600	9.47	0.60	3.40
CS23–DMF	610	9.04	0.61	3.37

4. Conclusion

Simple method is now available for the preparation of Ru(II) bipyridine analogous complex that is coordinated by 1-(2,4,6-trimethylbenzyl)-2-(2′-pyridyl)benzimidazole ligand. nc-DSC, sensitized with CS23 exhibits 3.40% electrical conversion efficiency which is nearly the same with reference ruthenium complex Z-907 under the same conditions. When compared with Z907, higher fill factor values are obtained with CS23.

Acknowledgements

We acknowledge the project support funds of Ege University and Helmholtz Centre Berlin for Materials and Energy, the State Planning Organization of Turkey (DPT), Alexander von Humboldt Foundation of Germany and the Scientific Research Council of Turkey (TUBITAK).

References

[1] Nazeeruddin MK, Angelis FD, Fantacci S, Selloni A, Viscardi G, Liska P, et al. Am Chem Soc 2005;127:16835–47.
[2] O'Regan B, Grätzel M. A low-cost, high-efficiency solar cell based on dye-sensitized colloidal TiO_2 films. Nature 1991;353:737–40.
[3] Kuang BD, Klein C, Ito S, Moser JE, Humphry-Baker R, Evans N, et al. High-efficiency and stable mesoscopic dye-sensitized solar cells based on a high molar extinction coefficient ruthenium sensitizer and nonvolatile electrolyte. Adv Mater 2007;19:1133–7.
[4] Grätzel M. Photoelectrochemical cells. Nature 2001;414:338–44.
[5] Jia WL, Hu YF, Gao J, Wang S. Linear and star-shaped polynuclear Ru(II) complexes of 2-(2-pyridyl)benzimidazolyl derivatives: syntheses, photophysical properties and red light-emitting devices. Dalton Trans 2006:1721–8.
[6] Yi H, Crayston JA, Irvine JTS. Ruthenium complexes of 2-(2-pyridyl) benzimidazole as photosensitizers for dye-sensitized solar cells. Dalton Trans 2003:685–91.
[7] Gobetto R, Caputo G, Garino C, Ghiani S, Nervi C, Salassa L, et al. Synthesis, electrochemical and electrogenerated chemiluminescence studies of ruthenium(II) bis(2,2_-bipyridyl){2-(4-methylpyridin-2-yl)benzo[*d*]-x-azole} complexes. Eur J Inorg Chem 2006:2839–49.
[8] Zhang XH, Kim SHo, Su Lee I, Ji Gao C, Ik Yang S, Ahn KH. Synthesis, photophysical and electrochemical properties of novel conjugated donor-acceptor molecules based on phenothiazine and benzimidazole. Bull Korean Chem Soc 2007;28(8):1389–95.
[9] Arslan H, VanDerveer D, Yasar S, Ozdemir I, Cetinkaya B. Dichlorido[1-(2-methylbenzyl)-3(η^6-2,4,6-trimethylbenzyl)-1 *H*-2,3-dihydrobenzimidazol-2-ylidene]ruthenium (II) dichloromethane solvate. Acta Cryst 2009;65:243–4.
[10] Åkermark B, Bjernemose J, Börje A, Chmielewski PJ, Paulsen H, Simonsen O, et al. Strain-induced substitutional lability in a Ru(II) complex of a hypodentate polypyridine ligand. Dalton Trans 2004:1215–20.
[11] Mitsopoulou CA, Veroni I, Philippopoulos AI, Falaras P. Synthesis, characterization and sensitization properties of two novel mono and bis carboxyl-dipyrido-phenazine ruthenium(II) charge transfer complexes. J Photochem Photobiology A Chem 2007;191:6–12.
[12] Yanagida M, Yamaguchi T, Kurashige M, Fujihashi G, Hara K, Katoh R, et al. Nanocrystalline solar cells sensitized with monocarboxyl or dicarboxyl pyridylquinoline ruthenium(II) complexes. Inorganica Chimica Acta 2003;351:283–90.
[13] Garelli N, Vierling P. Synthesis of new amphiphilic perfluoroalkylated bipyridines. J Org Chem 1992;57(11):3046–51.
[14] Wang P, Zakeeruddin SM, Comte P, Charvet R, Baker RH, Gratzel M. Enhance the performance of dye-sensitized solar cells by co-grafting amphiphilic sensitizer and hexadecylmalonic acid on TiO_2 nanocrystals. J Phys Chem B 2003;107:14336–41.
[15] Nazeeruddin MK, Kay A, Rodico I, Humphry-Baker R, M̈uller E, Liska P, et al. Conversion of light to electricity by cis-XzBis(2,2'-bipyridyl-4,4'-dicarboxylate)ruthenium(11) charge-Transfer Sensitizers (X = C1–, Br–, I–, CN–, and SCN–) on Nanocrystalline TiO_2 Electrodes. J Am Chem Soc 1993;115:6382–90.
[16] Nazeeruddin MK, Zakeeruddin SM, Lagref JJ, Liska P, Comte P, Barolo C, et al. Stepwise assembly of amphiphilic ruthenium sensitizers and their applications in dye-sensitized solar cell. Coordination Chem Rewiews 2004;248:1317–28.
[17] Sahin C, Tozlu C, Ocakoglu K, Zafer C, Varlikli C, Icli S. Synthesis of an amphiphilic ruthenium complex with swallow-tail bipyridyl ligand and its application in nc-DSC. Inorg Chim Acta 2008;361:671–6.
[18] Kuang BD, Klein C, Ito S, Moser JE, Humphry-Baker R, Zakeeruddin SM, et al. High molar extinction coefficient ion-coordinating ruthenium sensitizer for efficient and stable mesoscopic dye-sensitized solar cells. Adv Funct Mater 2007;17:154–60.
[19] Klein C, Nazeeruddin MK, Censo DD, Liska P, Grätzel M. Amphiphilic ruthenium sensitizers and their applications in dye-sensitized solar cells. Inorg Chem 2004;43:4216–26.
[20] Dittrich T, Neumann B, Tributsch H. Sensitization via reversibly inducible $Ru(dcbpyH_2)_2(NCS)_2$-TiO_2 charge-transfer complex. J Phys Chem C 2007;111:2265–9.
[21] Komiya R, Han L, Yamanaka R, Islam A, Mitate T. Highly efficient quasi-solid state dye-sensitized solar cell with ion conducting polymer electrolyte. J Photochem Photobiol A 2004;164:123–7.
[22] Y Liu, Hagfeldt A, Xiao XR, Lindquist SE. Investigation of influence of redox species on the interfacial energetics of a dye-sensitized nanoporous TiO_2 solar cell. Solar Energy Materials and Solar Cells 1998;55:267–81.
[23] Horiuchi T, Miura H, Sumioka K, Uchida S. High efficiency of dye-sensitized solar cells based on metal-free indoline dyes. J Am Chem Soc. 2004;126:12218–9.
[24] Galoppini E. Linkers for anchoring sensitizers to semiconductor nanoparticles. Coord Chem Rev 2004;248:1283–97.
[25] Kronik L, Shapira Y. Surface photovoltage phenomena: theory, experiment, and applications. Surface Sci Rep 1999;37:1–206.
[26] Kronik L, Shapira Y. Surface photovoltage spectroscopy of semiconductor structures: at the crossroads of physics, chemistry and electrical engineering. Surf Interface Anal 2001;31:954–65.
[27] Lenzmann F, Krueger J, Burnside S, Brooks K, Graetzel M, Gal D, et al. Surface photovoltage spectroscopy of dye-sensitized solar cells with TiO_2, Nb_2O_5, and $SrTiO_3$ nanocrystalline Photoanodes: indication for electron injection from higher excited dye States. JPhys Chem B 2001;105:6347–52.